Int. J. Heat Mass Transfer. Vol. 13, pp. 523–536. Pergamon Press 1970. Printed in Great Britain

THEORETICAL ANALYSIS OF BUBBLE DYNAMICS FOR AN ARTIFICIALLY PRODUCED VAPOR BUBBLE IN A TURBULENT STREAM

THEODORE T. ROBIN* and NATHAN W. SNYDER†

North American Rockwell Corporation, El Segundo, California

(*Received* 31 *December* 1968 *and in revised form* 28 *July* 1969)

Abstract—A mathematical model is given for an artificially produced vapor bubble growing on a surface and into a turbulent subcooled stream flowing parallel to the surface. This model was tested for steam injection through a 0·0135 in. hole in a stainless steel plate and into a water stream with Reynolds numbers from about $0{\cdot}9 \times 10^4$ to $2{\cdot}0 \times 10^5$, inlet bulk temperatures from 80 to 140°F, and near atmospheric pressure. Under these conditions, about 4000 bubbles per s were formed with a 0·02–0·03 in. radius. Heat transfer per bubble varied from about 1×10^5 to 5×10^5 Btu. Basic considerations of bubble dynamics for this model are discussed. Condensation at the bubble vapor–turbulent stream interface is a major component of this model. Subsequent diffusion of the associated latent heat into the turbulent stream was also important. Mathematical equations are given, and the method of solution is indicated. Agreement with experimental results demonstrates the validity of this model and the method of solution.

NOMENCLATURE

C_p, specific heat;
d, hydraulic diameter;
k; thermal conductivity;
$\dot{m}$; mass rate of evaporation or condensation;
M, molecular weight of fluid;
P, pressure of vapor in bubble;
P_∞, pressure of liquid in which bubble is growing;
P_E, Péclét number, Ud/ε_h';
Q, heat generation rate associated with condensation or evaporation;
r, radial coordinate;
r', dimensionless radial coordinate;
R, bubble radius;
$\dot{R}$, time derivative of R;
$\ddot{R}$, time derivative of $\dot{R}$;
R_0, universal gas constant;
t, time;
t', dimensionless time coordinate;
T, temperature;
T_f, initial temperature of cooling fluid;
T_{sat}, saturation temperature corresponding to the local fluid pressure;
T_{sur}, liquid surface temperature;
U, magnitude of velocity;
$\overline{V}$, velocity vector;
x, one dimensional coordinate;
y, $r' - \gamma$;
z, height above the channel wall;
α, accommodation coefficient defined as the ratio of the actual amount of condensation (or evaporation) to that predicted by kinetic theory;
γ, dimensionless radial coordinate for bubble wall;
$\dot{\gamma}$, $d\gamma/dt'$;
ε_h, eddy thermal diffusivity in turbulent flow;
ε_h', effective thermal diffusivity, $\dfrac{k}{\rho_1 C_p} + \varepsilon_h$;

* Atomics International, Division of North American Rockwell Corporation, Canoga Park, California.

† North American Rockwell Corporation, Executive Offices, El Segundo, California; Formerly Neely Professor, Georgia Institute of Technology, Atlanta, Georgia.

θ, angle;
μ, $-\cos\theta$;
ρ, vapor density;
ρ^*, vapor saturation density at T_{sur};
ρ_1, liquid density;
σ, surface tension;
τ_0, shear stress at the wall;
Φ, dimensionless temperature difference in liquid.

INTRODUCTION

HEAT transfer rates at the surface of vapor bubbles growing in a turbulent subcooled stream are enormous. Experiments [1–3] have shown that heat transfer coefficients of 300000 Btu/h ft^2 °F or higher are easily obtained for near atmospheric pressure systems. Latent heat associated with condensation on the bubble surface represents a large heat input to the liquid surrounding the bubble. Because no hydrodynamic boundary layer is present at the surface of the bubble, thermal resistance in the liquid is low corresponding to eddy diffusion. This mode of heat transfer is of interest because of its similarity with subcooled nucleate boiling in forced convection. Another application may be direct contact heat exchangers. By forcing vapor through a porous wall, the resulting bubbles will produce a large heat source in the turbulent core as vapor condenses. This process will bypass the high thermal resistant boundary layer. Main stream pressure drop should be similar to that of subcooled nucleate boiling. Theoretical analysis of this mode of heat transfer may yield insight useful in the design of novel heat exchangers.

In a previous paper [2] the mass transfer model [4] for a bubble in subcooled nucleate boiling was described in some detail. This process involves evaporation from a thin liquid film between the heated surface and the bubble vapor and the simultaneous condensation of vapor on the bubble cap which extends into the turbulent core of the stream. Experimental results with an artificial bubble, produced by injecting vapor through a small hole, indicate that mass transfer is potentially an important mode of heat transfer in subcooled nucleate boiling in forced convection [2]. However, this measurement alone does not determine the amount of condensation on the surface of a single bubble in subcooled nucleate boiling in forced convection. In that case, the vapor source —thin liquid film evaporation—is not the same as vapor injection through a small hole. To experimentally measure this condensation would be a difficult task. An accurate theoretical model for bubble dynamics in subcooled nucleate boiling would be useful in estimating the amount of condensation and other quantities which are difficult to measure. Validity of the general concepts and methods of solution should be demonstrated first. Such a test is possible using the experimental results of the artificial bubble experiment [2, 3] mentioned previously. Development of the model and a method of solution are given along with a comparison with experimental results. Methods developed here have been applied to the case of bubbles in subcooled nucleate boiling in forced convection, and the results are to be presented in a following paper.

GENERAL CONSIDERATIONS IN BUBBLE DYNAMICS

Mass transfer between liquid and vapor phase

Evaporation rate from a liquid surface into a vapor whose density is less than the saturation density corresponding to the liquid surface temperature is approximated by [5]:

$$\dot{m} = \alpha \left[\frac{R_0 T_{sur}}{2\pi M}\right]^{\frac{1}{2}} (\rho - \rho^*). \qquad (1)$$

If ρ^* is greater than ρ, equation (1) gives the magnitude of the condensation rate. Liquid surfaces associated with growing and collapsing bubbles are believed to be new and clean; thus, an accommodation coefficient of 1·0 was used in these calculations. There are two prime issues associated with the value of α determined by past experiments. These issues have been discussed by Hickman [6, 7] who performed clever

experiments to prove his point. First, when α was determined from evaporation of water by certain experimenters, they located their thermocouples below the interface and measured a temperature higher than that at the surface which was being cooled by the evaporation. Calculations of α were subsequently too low. Secondly, the surfaces were "old". That is, they had been in existence for many seconds or minutes. This invited either molecularly thin impurities to be lodged in the surface or for strong "potential wells" to form which also can result in low values of α. During boiling the surface forms in several μs and the entire bubble lifetime is 250–500 μs in forced convection subcooled nucleate boiling and several ms in pool boiling. Thus, evaporation and condensation occurs on surfaces that are very new and clean.

Dynamic equation for bubble radius

The Rayleigh equation [8] for growth of an isothermal bubble is given as:

$$\rho_1\{R\ddot{R} + (\tfrac{3}{2})(\dot{R})^2\} = P - P_\infty. \qquad (2)$$

In some cases an additional pressure term representing the effect of surface tension is subtracted from the right-hand side of equation (2). This term is $2\ \sigma/R$ where σ is the surface tension. The smallest value of R considered in this work was 0·001 in. and for the case of water, the missing term for the smallest radius has a value of approximately 1 psi. As R increases, this value decreases. $P - P_\infty$ may be as high as 20–30 psi initially and decreases as the bubble grows. Surface tension was neglected in this work.

General scheme of bubble dynamics

In this model, use was made of a control volume concept. The bubble was considered to be a hemisphere with its base on a flat surface. One boundary of the control volume was the interface between liquid and vapor at the surface of the hemisphere. The other boundary was the vapor–metal interfaces with a hole for vapor insertion at the base of the hemisphere.

At the bubble top, mass was allowed to cross the control surface by condensation or evaporation. If an amount of mass was condensed on the liquid surface during a time interval, the total amount of mass in the control volume was made smaller by that amount. However, the actual mass added to the liquid stream was neglected with respect to the total amount of mass in the stream and with respect to the dynamic motion of the stream (i.e. momentum effects were neglected). Also, heat conduction between vapor and liquid across the interface at the bubble top was neglected. However, the latent heat of condensation or evaporation was included as a source or sink in the heat balance of the liquid surrounding the bubble. The value for the latent heat was taken to be the saturation value corresponding to the bubble vapor density.

During most of the bubble lifetime, condensation at the bubble top provided a mass output from the bubble. In the experiment a mass input was provided by forcing a flow of steam through a tiny hole in the plate. Experimental values for the average mass input over the bubble life were determined. In the model for this case, the mass input to the control volume consisted of a constant amount of steam per unit time.

In the control volume the main concern was the total amount of mass inside the bubble, while in the surroundings the main concern was the thermal effect of the latent heat. Saturation was assumed for the state of the vapor in the bubble. The saturation density was calculated as the vapor mass present in the control volume divided by the volume. Pressure and temperature of the mass in the control volume was assumed uniform. Equation (1) governed the rate of mass flow across the control volume boundaries. Equation (2) determined the rate of growth of the bubble; the driving pressure differential was a function of time.

BUBBLE DYNAMICS FOR THE ARTIFICIAL BUBBLE

Description of bubble history and assumptions

During the bubble life, mass was added at a constant rate and removed by condensation on the bubble top. Change in the amount of mass in the bubble was determined by the difference between the mass input and the mass output and, in turn, affected bubble pressure. During the growth stage, pressure in the bubble was greater than local liquid pressure, and this caused the bubble to grow. However, as the surface area of the bubble grew larger, the mass output also increased because of the increasing area for condensation. Eventually, mass output exceeded mass input and the total mass in the bubble started to decrease. Also, as the bubble volume increased, the pressure in the bubble tended to decrease. At some point, the pressure became less than the local fluid pressure. These effects coupled with the dynamics expressed in equation (2) then led to a decreasing bubble radius and thus bubble collapse.

At any point during the bubble lifetime, the rate of mass output was controlled by the vapor density in the bubble and the liquid surface temperature. This temperature was controlled by the rate of heat input associated with condensation at the surface and the transfer of heat to the cooling stream. ρ^* in equation (2) was determined by the liquid surface temperature.

Assuming that the bubble was hemispherical during all of its lifetime is not completely correct. However, high speed photographs [3] show that this is not too bad over most of the bubble lifetime. During initial and final stages of the bubble lifetime, the shape of the bubble was not that of a hemisphere. Since the steam came through a hole in the heated plate with a diameter of 0·0135 in., the initial interface between liquid and vapor was a flat circular disk. This was transformed into a roughly hemispherical surface at some later time. Because of the mathematical complexity of describing such a transformation, the initial bubble radius was assumed to be 0·013 in.

Establishing the vapor state and liquid temperature distribution at the initial time was required. Pressure was the most critical item concerning the vapor state. For a bubble in real boiling, the initial radius is usually small and the initial pressure is usually high (possibly as much as 20–30 psia higher than ambient liquid pressure). However, as the bubble grows, pressure in the bubble approaches ambient liquid pressure. In the experimental case, 0·013 in was usually about 50 per cent of the maximum radius. Thus, bubble pressure was chosen slightly larger than local stream pressure. First, local liquid pressure near the bubble site for the run under consideration was determined and then the corresponding saturation temperature. A temperature slightly greater than this value was chosen as the vapor temperature in the bubble and the vapor was assumed saturated at this temperature. This made the bubble pressure slightly larger than local liquid pressure.

As a first approximation to the liquid temperature distribution at the beginning of the solution, a step distribution was assumed. That is, the temperature of a thin shell of liquid around the bubble was assumed to be equal to the bubble vapor temperature at that time. The remainder of the liquid was assumed to be equal to the inlet temperature of the cooling fluid as determined in the experiment. Shell thickness was chosen so as to account for the heat input to the bubble wall during growth from the flat disk interface to the hemispherical interface with a radius of 0·013 in. This was done by first assuming the time required to grow from a flat disk to a hemisphere. Heat input during this time was calculated by multiplying the time interval by the rate of heat input which was a constant. $Q = mC_P\Delta T$ was used to calculate the mass of liquid which would experience a temperature rise corresponding to the difference in temperature of the thin shell and the inlet temperature. Knowing the density of the liquid, the volume was then calculated from the known mass. Finally, since the surface area of the bubble was known, the shell thickness was obtained.

Initial values for $\dot{R}$ and $\ddot{R}$ were also required. $\ddot{R}$ was assumed to be zero, and then $\dot{R}$ was calculated using equation (2). A uniform velocity profile was assumed for the stream in which the bubble was growing. In reality it was that corresponding to fully developed turbulent flow for the high velocity cases. In those cases, the boundary layer was of the order of 10^{-3} in. and, since the bubble radius was usually large compared to this value, the uniform velocity assumption was justified. Experimental mean velocity was used as the magnitude of the uniform velocity. However, for the low velocity cases, the velocity profile was probably more parabolic. Nevertheless, a uniform velocity, equal to the mean velocity, was assumed here. For high pressure applications, 2000 psi, and low velocities, a more accurate description of the velocity and initial temperature profiles will probably be required.

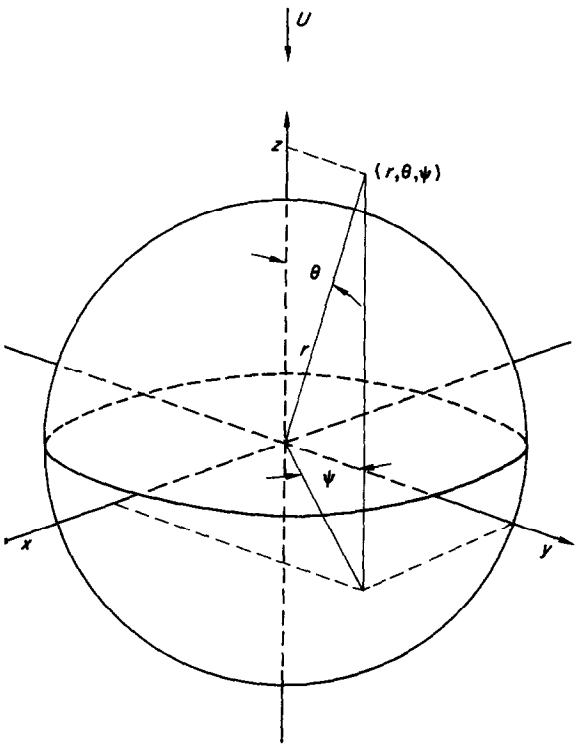

FIG. 1. Equivalent coordinate system for the single bubble case.

Heat diffusion from bubble surface

By making the bubble spherical rather than hemispherical and making the mass input rate twice as great as the actual rate, the mathematical heat diffusion problem is similar to a case considered by Wittke [9]. In his case a uniform flow of liquid impinged on a spherical bubble as shown in Fig. 1. Since no heat flow occurred in the ψ direction, the case under consideration here and his case were similar under changes stated above. For example, the heated plate might be considered to be the x–z plane. (Note that the heat transfer from the heated plate to the fluid by convection was neglected.) The heat diffusion equation to be solved was that derived by Wittke plus a heat generation term:

$$\frac{\partial T}{\partial t} + \left[-U\left(1 - \frac{R^3}{r^3}\cos\theta\right) + \frac{R^2\dot{R}}{r^2}\right]\frac{\partial T}{\partial r} + \frac{U}{r}\left(1 + \tfrac{1}{2}\frac{R^3}{r^3}\right)\sin\theta\frac{\partial T}{\partial \theta} = \varepsilon_h'\left(\frac{\partial^2 T}{\partial r^2} + \frac{2}{r}\frac{\partial T}{\partial r} + \frac{1}{r}\frac{\partial^2 T}{\partial \theta^2} + \frac{\cot\theta}{r^2}\frac{\partial T}{\partial \theta}\right) + \frac{Q}{\rho_1 C_p} \tag{3}$$

where $T = T(t, r, \theta)$.

Heat generation rate will be zero everywhere except in a thin shell surrounding the bubble. Here the latent heat of condensation (or vaporization) will be considered a heat source (or sink) uniformly distributed throughout the shell. The numerical approach here is similar to one considered by Dusinberre [10] for radiant heating. Under this procedure the boundary condition for the vapor liquid interface is

$$\left.\frac{\partial T}{\partial r}\right| = 0$$

$$r = R.$$

The other boundary condition is

$$\left.\frac{\partial T}{\partial r}\right| = 0$$

$$r = R_{\max}$$

where $R_{\max}$ is a substantial distance from the bubble surface. Boundary conditions in the θ direction are

$$\left.\frac{\partial T}{\partial \theta}\right| = 0 \qquad \text{and} \qquad \left.\frac{\partial T}{\partial \theta}\right| = 0$$

$$\theta = 0 \qquad\qquad \theta = 180^\circ.$$

Initial temperature distribution was described previously. Now let

$$\Phi = (T - T_f)/(T_{\text{sat}} - T_f) \tag{4}$$

where T_f is the initial temperature of the cooling fluid and T_{sat} is the saturation temperature corresponding to the local fluid pressure, P_∞. Also let

$$t' = 4\frac{\varepsilon_h'}{d^2}t \tag{5}$$

where d is the equivalent hydraulic diameter of the channel. Let

$$r' = \frac{2r}{d} \qquad \text{and} \qquad \gamma = \frac{2R}{d}. \tag{6}$$

Also define a Péclét number

$$P_E = Ud/\varepsilon_h'. \tag{7}$$

Now using equations (4)–(7), equation (3) becomes:

$$\frac{\partial\Phi}{\partial t'} - \frac{P_E}{2}\left(1 - \frac{\gamma^3}{r'^3}\right)\cos\theta\frac{\partial\Phi}{\partial r'} + \dot\gamma\frac{\gamma^2}{r'^2}\frac{\partial\Phi}{\partial r'} + \frac{P_E}{2}\frac{1}{r'}\left(1 + \tfrac{1}{2}\frac{\gamma^3}{r'^3}\right)\sin\theta\frac{\partial\Phi}{\partial\theta} = \frac{\partial^2\Phi}{\partial r'^2} + \frac{2}{r'}\frac{\partial\Phi}{\partial r'} + \frac{1}{r'^2}\frac{\partial^2\Phi}{\partial\theta^2} + \frac{\cot\theta}{r'^2}\frac{\partial\Phi}{\partial\theta} + \frac{Q(d)^2}{4\varepsilon_h'\rho_1 C_P(T_{\text{sat}} - T_f)} \tag{8}$$

where $\dot\gamma = \mathrm{d}\gamma/\mathrm{d}t'$.

Also with the transformations,

$$y = r' - \gamma \qquad \text{and} \qquad \mu = -\cos\theta \tag{9}$$

equation (8) becomes:

$$\frac{\partial\Phi}{\partial t'} - \dot\gamma\left[1 - \frac{1}{\left(1 + \frac{y}{\gamma}\right)^2}\right]\frac{\partial\Phi}{\partial y} + \frac{P_E}{2}\mu\left[1 - \frac{1}{\left(1 + \frac{y}{\gamma}\right)^3}\right]\frac{\partial\Phi}{\partial y} + \frac{P_E}{2}\frac{(1-\mu^2)}{\gamma\left(1 + \frac{y}{\gamma}\right)}\left[1 + \frac{1}{2\left(1 + \frac{y}{\gamma}\right)^3}\right]\frac{\partial\Phi}{\partial\mu} = \frac{\partial^2\Phi}{\partial y^2} + \frac{2}{\gamma\left(1 + \frac{y}{\gamma}\right)}\frac{\partial\Phi}{\partial y} + \frac{(1-\mu^2)}{\gamma^2\left(1 + \frac{y}{\gamma}\right)^2}\frac{\partial^2\Phi}{\partial\mu^2} - \frac{2\mu}{\gamma^2\left(1 + \frac{y}{\gamma}\right)^2}\frac{\partial\Phi}{\partial\mu} + \frac{Q(d)^2}{4\varepsilon_h'\rho_1 C_P(T_{\text{sat}} - T_f)}. \tag{10}$$

Numerical approximation to equation (10) is developed in [2]. $\partial\Phi/\partial y$ and $\partial\Phi/\partial\mu$ on the left-hand side of equation (10) could not be represented with the same numerical approximation as those quantities on the right-hand side, possibly caused by the assumed initial temperature distribution (see Appendix A).

Method of advancing numerical solution

After the solution had been advanced up to a time t, the following quantities were known:

1. State of bubble vapor (density and pressure).
2. R, $\dot R$, $\ddot R$ and bubble volume.
3. Amount of mass in the bubble.
4. Liquid temperature at the vapor–liquid interface.
5. Liquid temperature distribution.

To advance the solution an increment of time, the following procedure was used:

1. Since R, $\dot R$, $\ddot R$ and the bubble vapor pressure were known, change in R, $\dot R$, $\ddot R$ was calculated

with the aid of equation (2) and a Taylor series expansion for $\dot{R}$ and $\ddot{R}$ (see Appendix B).

2. Equation (1) was used to calculate the amount of vapor condensed. This involved calculating the saturation vapor density corresponding to the known liquid surface temperature.* Using this value and the known value of the bubble vapor density, the amount condensed was calculated.

3. New total mass in the bubble was calculated by adding to the old total mass the difference between the amount condensed and the amount added by the constant rate of mass addition.

4. Volume was calculated using the new value of R found in step 1. This was divided into the new mass found in step 3, and the result was the new density. Under the assumption that the vapor in the bubble was saturated, the new pressure was determined from the steam tables.

5. Latent heat represented by the condensed steam was then used along with the numerical approximation to equation (10) to calculate the new surface temperature and the new liquid temperature distribution.

Following this procedure, the variables were determined over the life of the bubble.

COMPARISON OF MODEL AND EXPERIMENTAL RESULTS

Predictions from the above model were compared with experimental data for steam injection through 0·0135 in. hole in a heated plate and into a subcooled stream of water flowing parallel to the heated plate. The experimental data are presented and discussed in [2, 3]. Comparison with the model was based on maximum bubble volume (radius). Maximum bubble volume was determined from high speed motion picture film. Bubble frequency was about 4000 bubbles per s and camera speed was 8000 frames per s. Thus, only two or three frames were available per bubble. Maximum bubble volume was plotted as a function of time for about 100 frames. The largest bubble observed was selected as the maximum bubble size. Since the bubble radius is large over a significant portion of bubble life, several frames should contain bubbles very close to maximum size. The largest error involved was caused by the assumption of hemispherical shape and the fact that the bubble was observed in only one plane. Overall error in bubble volume was estimated to be ± 10 per cent. Bubble frequency (lifetime) was also determined from the plot of the high speed motion picture film. In a sequence of three frames, the bubble was observed to be: (1) in initial growth; (2) near maximum size; and (3) in final state of collapse. Thus, bubble lifetime was approximately two times the time interval between frames. Error in bubble lifetime measurement was estimated to be ± 17 per cent. Because of the slow framing rate, no attempt was made to determine an experimental radius vs. time curve.

One unknown in the mathematical model is the value of ε_h' that is effective in the liquid surrounding the bubble. ε_h' was assumed, and the choice which resulted in agreement between theory and experimental results was noted. Bubble radius as a function of time as predicted by the theoretical model is shown in Fig. 2 for

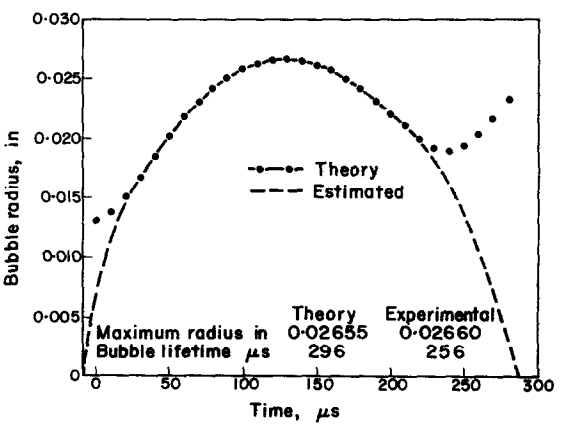

FIG. 2. Bubble radius as a function of time for run no. 7.

* The variation in T_{sur} with θ was taken into account in using equation (1). The bubble surface was divided into a number of segments for the numerical solution and equation (1) was applied to each segment individually.

the conditions of experimental run no. 7 (see [3]; the pertinent variables were: mass input rate = 0·692 lb/h, $U = 12{\cdot}0$ ft/s, $T_f = 110°F$, and $P_\infty = 16{\cdot}0$ psia). ε_h' was 1·2 ft^2/h, and this choice resulted in a maximum radius of 0·0266 in. as compared to the experimental value of 0·0266 in. Predicted value and observed value of the bubble lifetime are 286 and 256 μs, respectively. This comparison is not as good, but it is within experimental error.

Near the beginning and end of the bubble life, the theoretical model did not correctly predict the physical situation. It was realized that the model developed would be most accurate only when the bubble size is large. Because the bubble size was large during most of its lifetime, the theoretical model is acceptable for the present even with the poor prediction for small bubble radii.*

Another source of inaccuracy in the solution to the model is the use of equation (2) for bubble growth in a uniform velocity field. Assuming bubble remains spherical in the velocity field (as in [9]) equation (2) would have additional terms of the order of $\frac{1}{2}\rho U^2$. This term would be negligible for the low velocity cases. For $U = 1{\cdot}9$ ft/s, $\frac{1}{2}\rho U^2 = 0{\cdot}03$ psi and for $U = 12$ ft/s, $\frac{1}{2}\rho U^2 = 1{\cdot}0$ psi. However, for $U = 25{\cdot}5$ ft/s, $\frac{1}{2}\rho U^2 = 4{\cdot}5$ psi which is about 25 per cent of P_∞.

From the experimental data [3], an increase in the velocity from 12·0 to 25·5 ft/s resulted in a 25 per cent decrease in maximum bubble radius from 0·0266 to 0·020 in., other variables held essentially constant. Most of this decrease is attributed to an increase in ε_h and a faster movement of colder fluid over the bubble (both increasing the condensation rate). The theoretical maximum bubble radius was a strong function of the assumed value of ε_h; a 33 per cent change in theoretical maximum bubble radius could be caused by a 5 per cent change in ε_h (see curves 2 and 3 of Fig. 12 of [2] or of Fig. 4 of [12]). Thus, even if the full 25 per cent change in maximum bubble radius (caused by changing velocity from 12 to 25·5 ft/s) is attributed to $\frac{1}{2}\rho U^2$, only a 5 per cent change in the reported value of ε_h would be required to have agreement between theoretical and experimental maximum bubble radius. In the present application, inaccuracies because of the use of equation (2) in a uniform velocity field, should result in errors in the reported values of ε_h of 5 per cent or less. In light of the 10 per cent error in the experimental data for maximum bubble radius, use of equation (2) was acceptable. Also, because the bubble surface was usually not smooth, a more detailed analysis does not seem warranted.

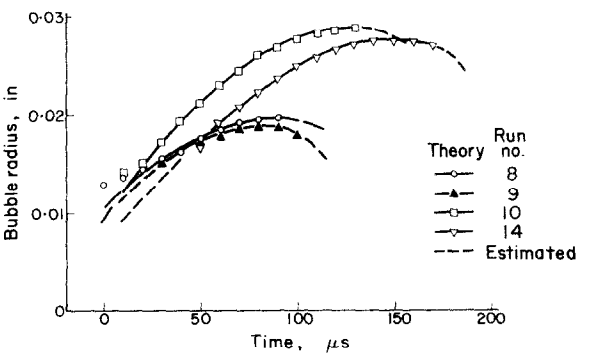

FIG. 3. Bubble radius as a function of time for runs no. 8–11.

Bubble radius as a function of time (up to the maximum bubble radius) for several other experimental runs is shown in Fig. 3. Some pertinent information is tabulated in Table 1. Since the velocity was the same for runs 8, 9 and 10, the value for the effective thermal diffusivity was expected to be approximately the same

* Theoretical bubble radius shown in Fig. 2 does not completely collapse. After an initial collapse, the bubble enters a new growth phase. This behavior does not indicate that the radius vs. time solution is unstable. The observed behavior is caused by the assumption of a constant rate of vapor input to the bubble. During the collapse phase, this constant input causes a rise in bubble pressure as shown in Fig. 6. The resulting bubble growth phase is in accord with the assumed dynamic equation for bubble radius, equation (2). $P - P_\infty$ becomes large enough to initiate a new growth phase.

value for all three runs. Only the change in the cooling fluid temperature and that in the vapor input rate would change the experimentally observed maximum radius in runs 9 and 10 from the value observed in run 8. ε'_h, which yielded agreement between the theoretically predicted maximum bubble radius and that experimentally observed for run 8, was used in the model for runs 9 and 10. In this way the consistency of the theoretical model with the actual physical phenomenon could be determined. For run 9, the predicted maximum radius differed by only +8 per cent from the observed value, while for run 10 the difference was only −8 per cent.

Values of ε'_h which yield agreement between experiment and theory are plotted as points in Fig. 4 as a function of the cooling stream velocity. Since the flow condition was that of fully developed turbulent flow, the theoretical value of the eddy diffusivity for momentum transfer in fully developed turbulent flow in a pipe at a distance of 0·02 in. from the wall is shown for comparison. This theoretical value

Table 1. *Results of runs no.* 8, 9, 10 *and* 14 (*see* [3])

Run	T_f (°F)	U (ft/s)	ε'_h (ft²/h)	Maximum bubble radius Model (in.)	Maximum bubble radius Experimental (in.)	Deviation (%)
8	110	25·5	3·00	0·01976	0·0200	− 1
9	80	25·5	3·00	0·01857	0·0172	+ 8
10	140	25·5	3·00	0·02893	0·0314	− 8
14	110	1·9	0·06	0·02763	0·0280	− 1

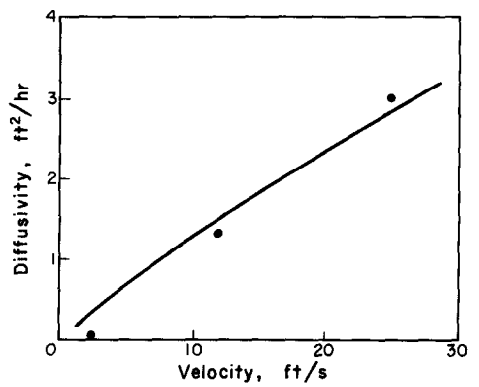

FIG. 4. Effective thermal diffusivity as a function of cooling stream velocity: solid line is theoretical value for eddy diffusivity for fully developed turbulent flow, 0·02 in. from wall.

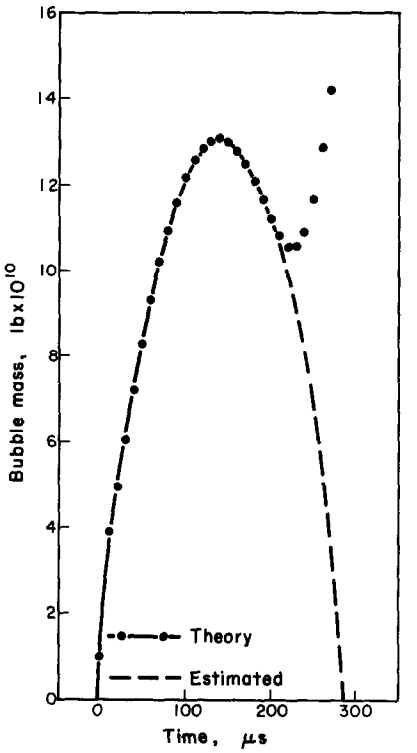

FIG. 5. Bubble mass as a function of time for run no. 7.

was calculated using the following expression [11]:

$$\varepsilon_m = (0{\cdot}4)^2 z^2 \left(1 - \frac{2z}{d}\right)\frac{2{\cdot}5}{z}\sqrt{\left(\frac{\tau_0}{\rho_1}\right)}. \qquad (11)$$

Good agreement between ε_h' and ε_m offers a significant degree of confidence in the concepts and methods used in the solution to this model.

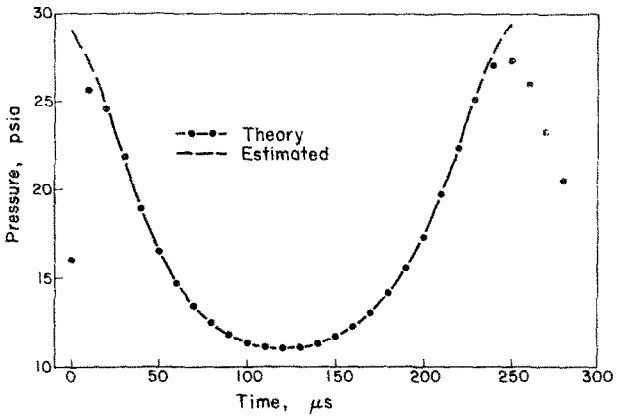

FIG. 6. Bubble pressure as a function of time for run no. 7.

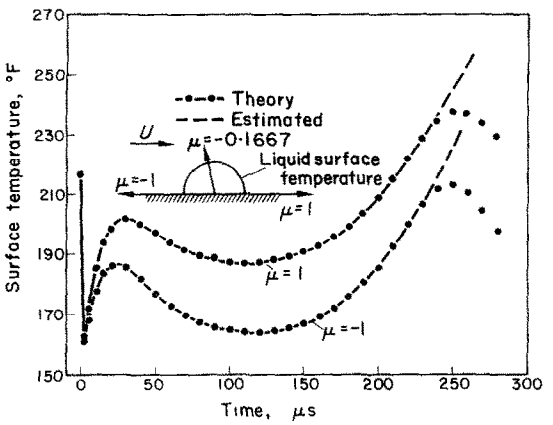

FIG. 7. Liquid surface temperature as a function of time for run no. 7.

A number of variables were recorded for run 7 in order to characterize this solution to the theoretical model. Again, it is emphasized that because of the assumptions concerning the initial conditions, the solution is most valid for large values of R. Hence, the behavior indicated in the following plots for times $< \sim 30$ μs and > 200 μs are certainly questionable. Figures 5–7 represent the bubble mass, the bubble pressure, and the liquid surface temperature as functions of time, respectively. Figures 8–13 represent the

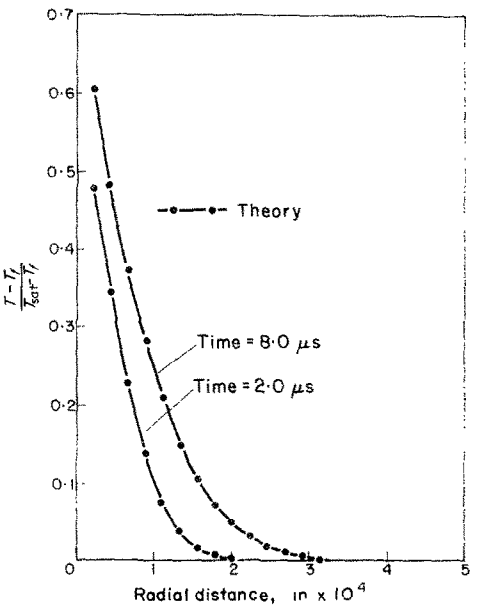

FIG. 8. Dimensionless temperature difference for the cooling liquid as a function of radial distance from the bubble surface for $\mu = -1$ (upstream direction) for run no. 7.

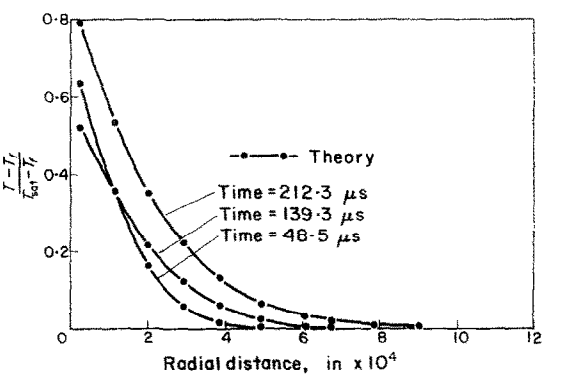

FIG. 9. Dimensionless temperature distribution for the cooling liquid as a function of radial distance from the bubble surface for $\mu = -1$ (upstream direction) for run no. 7.

temperature distribution in the liquid surrounding the bubble at various times during its life. Liquid surface temperature as a function of μ at various times during the bubble life is shown in Fig. 14. To be noted in Fig. 14 is the fact that the temperature of the liquid surface varied at times as much as 20° F from $\mu = -1$ to $\mu = +1$. Also, the temperature distribution in the upstream direction (see Fig. 9) was much steeper than in the downstream direction (see Fig. 13). These results are reasonable; since cold fluid comes from the upstream direction, the surface

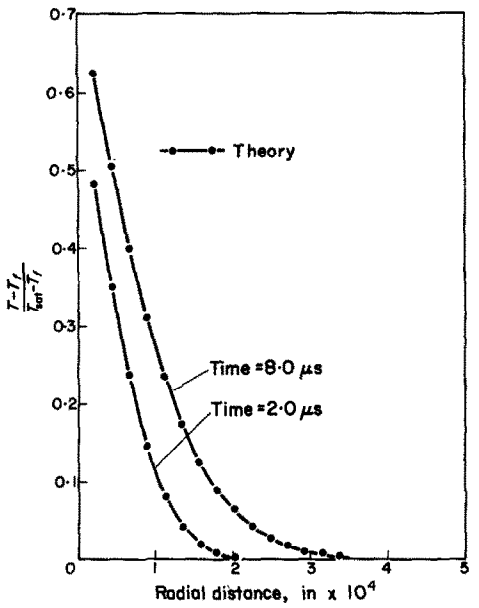

FIG. 10. Dimensionless temperature distribution for the cooling liquid as a function of radial distance from the bubble surface for $\mu = -0{\cdot}1667$ for run no. 7.

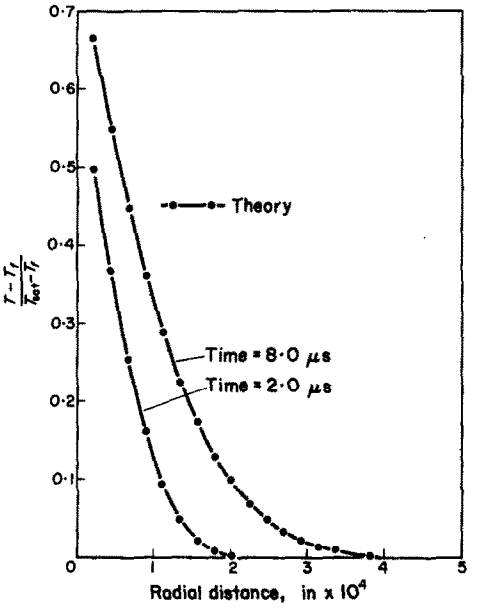

FIG. 12. Dimensionless temperature distribution for the cooling liquid as a function of radial distance from the bubble surface for $\mu = +1$ (downstream direction) for run no. 7.

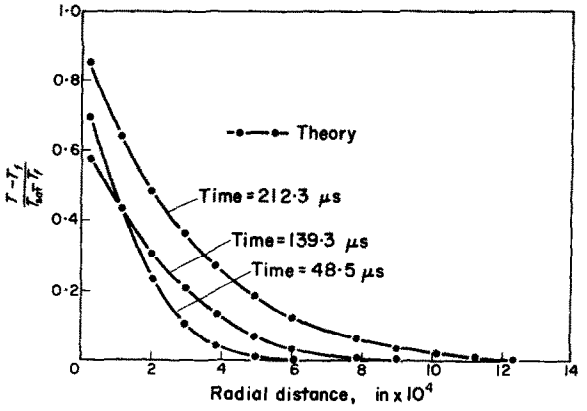

FIG. 11. Dimensionless temperature distribution for the cooling liquid as a function of radial distance from the bubble surface for $\mu = -0{\cdot}1667$ for run no. 7.

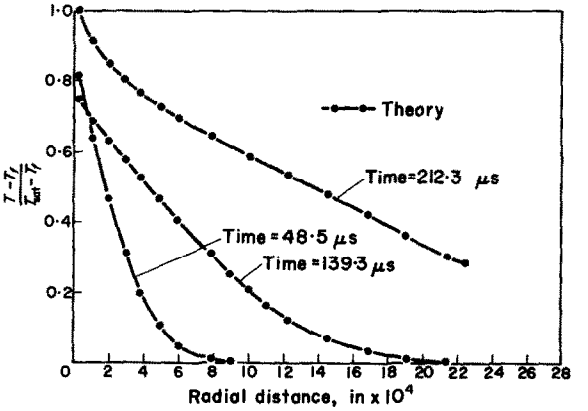

FIG. 13. Dimensionless temperature distribution for the cooling liquid as a function of radial distance from the bubble surface for $\mu = +1$ (downstream direction) for run no. 7.

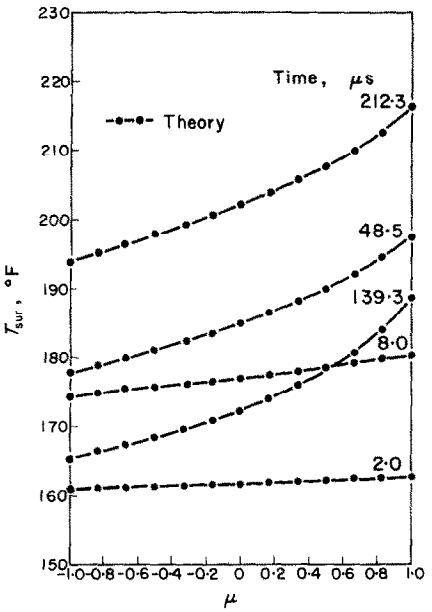

FIG. 14. Liquid surface temperature as a function of μ for run no. 7.

temperature of the fluid at this end should be coldest. Also, as the fluid moves over the bubble, its temperature should increase due to the latent heat of condensation. Experimental values for the relations indicated in the above plots would be useful.

CONCLUSIONS

1. Effective thermal diffusivity near a single steam bubble growing in a fully developed turbulent stream is approximately the value of the eddy diffusivity for momentum transfer about one bubble radius from the wall. This value ranged from about 0·1 to 3·0 ft^2/h for the case considered.

2. Coupling of equations (1) and (2) with a heat and mass balance of the bubble system appears to be sufficiently accurate for predicting bubble dynamics.

3. This model may be used, as a first approximation, to predict the rate of heat transfer in possible heat exchanger applications using this mode of heat transfer.

REFERENCES

1. S. G. BANKOFF and J. P. MASON, Heat transfer from the surface of a steam bubble in turbulent subcooled liquid stream, *A.I.Ch.E.Jl.* **8**, 30 (1962).
2. N. W. SNYDER and T. T. ROBIN, The mass transfer model in subcooled nucleate boiling, *J. Heat Transfer* **91C**, 404 (1969).
3. T. T. ROBIN. Mass transfer effects in subcooled nucleate boiling, Ph.D. Thesis, Georgia Inst. of Technology (1966).
4. S. G. BANKOFF, W. J. COLAHAN, JR and D. R. BARTZ, Summary of conference on bubble dynamics and boiling heat transfer held at the Jet Propulsion Laboratory, Jet Propulsion Laboratory Memo. 20–137, June 14 and 15 (1956).
5. E. H. KENNARD, *Kinetic Theory of Gases*. McGraw-Hill (1938).
6. K. C. D. HICKMAN and D. J. TREVOY, Evaporation from liquids in high vacuum, *Chem. Engng Prog.* **49**, 105–109 (1953).
7. K. HICKMAN, Evaporation coefficients of liquids, 1st International Symposium on Water Desalination, SWD/27 (1965).
8. H. LAMB, *Hydrodynamics* 6th edn., p. 122. Cambridge (1932).
9. D. D. WITTKE, Collapse of vapor bubbles with translatory motion, Ph.D. Thesis, University of Illinois (1965).
10. G. M. DUSINBERRE, *Numerical Analysis of Heat Flow*. McGraw-Hill (1949).
11. B. A. BAKHMETEFF, *The Mechanics of Turbulent Flow*. Princeton Univ. Press, Princeton, N.J. (1941).

APPENDIX A

$\partial\Phi/\partial y$ and $\partial\Phi/\partial\mu$ on the left-hand side of equation (10) could not be approximated in the same manner as those quantities on the right-hand side. The presence of these derivatives on the right-hand side was caused by heat conduction, whereas, on the left-hand side the reason was fluid motion. The cause which would not allow the two cases to be treated in a similar manner can be explained by considering a simplified one-dimensional problem of the same nature.

Consider one-dimensional flow of liquid in the $+x$ direction (see Fig. 15) with a velocity of U ft/s with respect to the coordinate system. Now the equation under consideration is:

$$\frac{\partial T(x,t)}{\partial t} + \bar{V}\cdot\nabla T(x,t) = \varepsilon_h'\nabla^2 T(x,t) \qquad (12)$$

where $\bar{V}$ is the velocity vector. The term $\bar{V}\cdot\nabla T$ is caused by bulk fluid transport. Equation (12) is equivalent to

$$\frac{\partial T(x,t)}{\partial t} + U\frac{\partial T(x,t)}{\partial x} = \varepsilon_h'\frac{\partial^2 T(x,t)}{\partial x^2}. \qquad (13)$$

For this illustration, ε_h' is assumed to be zero and equation (13) becomes:

$$\frac{\partial T(x,t)}{\partial t} + U\frac{\partial T(x,t)}{\partial x} = 0. \tag{14}$$

The usual approximations to these derivatives are

$$\frac{\partial T}{\partial t} = \frac{T_{J,n+1} - T_{J,n}}{Dt}$$

and

$$\frac{\partial T}{\partial x} = \frac{T_{J+1,n} - T_{J-1,n}}{2Dx}$$

where J relates to the space coordinate, n relates to time, Dx is an increment of x, and Dt is an increment of t. Using these equations, (14) becomes:

$$\frac{T_{J,n+1} - T_{J,n}}{Dt} + U\frac{T_{J+1,n} - T_{J-1,n}}{2Dx} = 0$$

or

$$T_{J,n+1} = T_{J,n} + \frac{U}{2}\frac{Dt}{Dx}T_{J-1,n} - \frac{U}{2}\frac{Dt}{Dx}T_{J+1,n}. \tag{15}$$

Now assume the initial condition such that $T_{J,0} = T_{J-1,0} \ll T_{J+1,0}$. In this case, equation (15) indicates that the higher the value of $T_{J+1,n}$, the lower the temperature at J will be at

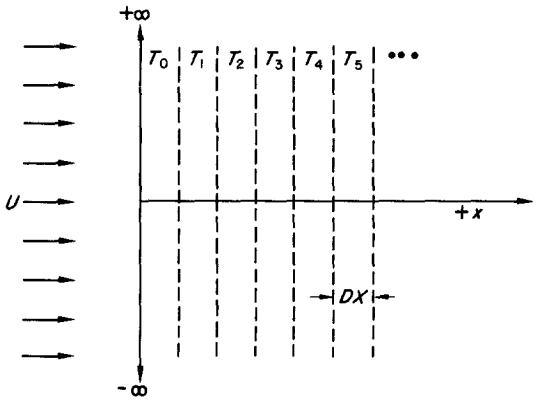

FIG. 15. Coordinate system for the one-dimensional illustration.

time $(n+1)\cdot Dt$. Physically, this is impossible. Since U is in the $+x$ direction and since ε_h' equals zero, T_{J+1} at any time should have no effect on T_J. The error in the above derivation arises from the approximation of $\partial T/\partial x$. A correct one for this case is:

$$\frac{\partial T}{\partial x} = \frac{T_{J,n} - T_{J-1,n}}{Dx}.$$

Using this, the equivalent of equation (15) is:

$$T_{J,n+1} = T_{J,n} + U\frac{Dt}{Dx}T_{J-1,n} - U\frac{Dt}{Dx}T_{J,n}. \tag{16}$$

Equation (16) is logically correct. Consider the initial condition: $T_{J,0} \gg T_{J-1,0}$. As fluid of high temperature, $T_{J,0}$, leaves cell J to go into cell $J+1$ and as fluid of low temperature, $T_{J-1,0}$, leaves cell $J-1$ to go into cell J, the resulting temperature of the homogenized fluid in cell J is lower than $T_{J,0}$. Furthermore, the higher the value of $T_{J-1,0}$, and the lower the value of $T_{J-1,0}$, the larger would be the change in temperature of location J. Thus, derivatives arising due to the transport of bulk fluid must be treated in a non-conventional manner for the present problem.

During the initial attempt to solve equation (10), several methods were used. All attempts used the conventional numerical approximations to the derivatives $\partial\Phi/\partial y$ and $\partial\Phi/\partial\mu$, regardless of their origin. Implicit, explicit and a combination implicit–explicit were all tried. However, an instability in the predicted temperature distribution persisted. Reasoning similar to that illustrated above in the one-dimensional case led to a representation of these terms which produced a stable solution.

APPENDIX B

Numerical approximations for R, $\dot{R}$ and $\ddot{R}$ are indicated below:

$$R_{n+1} = R_n + \dot{R}_n \cdot Dt + \ddot{R}_n\frac{Dt^2}{2}$$

$$\dot{R}_{n+1} = \dot{R}_n + R_n \cdot Dt$$

$$\ddot{R}_{n+1} = \left[\frac{P_n - P_\infty}{\rho_1} - \tfrac{3}{2}(\dot{R}_n)^2\right]\frac{1}{R_n}$$

where R_n indicates the bubble radius at time $n \cdot Dt$.

ANALYSE THEORIQUE DE LA DYNAMIQUE DES BULLES POUR UNE BULLE DE VAPEUR PRODUITE ARTIFICIELLEMENT DANS UN ECOULEMENT TURBULENT

Résumé—On donne un modèle mathématique pour une bulle de vapeur produite artificiellement croissant sur une surface et à l'intérieur d'un écoulement turbulent sous-refroidi parallèle à la surface. Ce modèle a été essayé pour l'injection de vapeur à travers un trou de 0,343 mm de diamètre dans une plaque d'acier inoxydable et dans un écoulement d'eau avec des nombres de Reynolds allant d'environ $0{,}9 \cdot 10^4$ à $2 \cdot 10^5$,

des températures globales d'entrée de 26,7 à 60°C et environ à la pression atmosphérique. Sous ces conditions, environ 4000 bulles par seconde étaient formées avec un rayon de 0,50 à 0,75 mm de diamètre. Le transport de chaleur par bulle variait d'environ 10^{-2} à $5 . 10^{-2}$ Joule. Des considérations de base de la dynamique des bulles pour ce modèle sont discutées. La condensation à l'interface bulle de vapeur—écoulement turbulent est un constituant important de ce modèle. La diffusion qui s'ensuit de la chaleur latente associée dans l'écoulement turbulent était également importante. Les équations mathématiques sont données et la méthode de résolution est indiquée. L'accord avec les résultats expérimentaux démontre la validité de ce modèle et de la méthode de résolution.

THEORETISCHE UNTERSUCHUNG DER BLASENDYNAMIK FÜR EINE KÜNSTLICH ERZEUGTE DAMPFBLASE IN TURBULENTER STRÖMUNG

Zusammenfassung—Es wird ein mathematisches Modell angegeben für eine künstlich erzeugte Dampfblase, die auf einer Oberfläche in einen turbulenten unterkühlten Strom, der parallel zur Oberfläche fliesst, hineinwächst. Dieses Modell wurde getestet für Dampfinjektion durch eine 0,343 mm Bohrung in einer Platte aus rostfreiem Stahl in einen Wasserstrom mit Reynolds-Zahlen von $0,9 \times 10^4$ bis $2,0 \times 10^5$ und Einlass-Badtemperaturen von 27 bis 60°C, in der Nähe des atmosphärischen Druckes. Unter diesen Bedingungen wurden etwa 4000 Blasen pro Sekunde gebildet mit 0,5–0,8 mm Radius. Die Wärmemenge pro Blase variierte von etwa 0,01 bis 0,053 J. Grundlegende Betrachtungen der Blasendynamik für dieses Modell wurden diskutiert. Die Kondensation an der Blasengrenze zwischen Dampf und turbulenter Strömung ist eine Hauptkomponente des Modells. Anschliessende Diffusion der damit verbundenen Verdampfungswärme in die turbulente Strömung war ebenfalls wichtig. Mathematische Gleichungen wurden aufgestellt, und die Lösungsmethode ist angedeutet. Übereinstimmung mit experimentellen Ergebnissen zeigt die Gültigkeit dieses Modells und der Lösungsmethode.

ТЕОРЕТИЧЕСКИЙ АНАЛИЗ ДИНАМИКИ ПУЗЫРЬКА – ИСКУССТВЕННО СОЗДАННОГО ПУЗЫРЬКА ПАРА В ТУРБУЛЕНТНОМ ПОТОКЕ

Аннотация—Приводится математическая модель искусственно создаваемого пузырька, растущего на поверхности и в параллельном этой поверхности турбулентном потоке переохлажденной жидкости. Эта модель проверялась для случая вдува пара через 0.0135 дюйм. отверстие в пластине из нержавеющей стали в поток воды с числами Рейнольдса от 0.9×10^4 до 2.0×10^5, температурой ядра потока на входе от 80 до 140°ф и давлением, близков к атмосферному. При этих условиях в секунду образовывались около 4000 пузырьков радиусом 0,02–0,03 дюйма. Теплообмен, приходящийся на один пузырек, составлял от 1×10^{-5} до 5×10^{-5} БТЕ. Рассматриваются основные соображения относительно динамики пузырьков для этой модели. Основным компонентом модели является конденсация на поверхности раздела пузырек пара — турбулентный поток. Немаловажна и диффузия связанного скрытого тепла в турбулентный поток. Получены математические уравнения и указаны методы решения. Соответствие с экспериментальными результатами свидетельствует о пригодности этой модели и метода решения.